Article

Cell

Mechanisms of Anion Conduction by Coupled Glutamate Transporters

Graphical Abstract

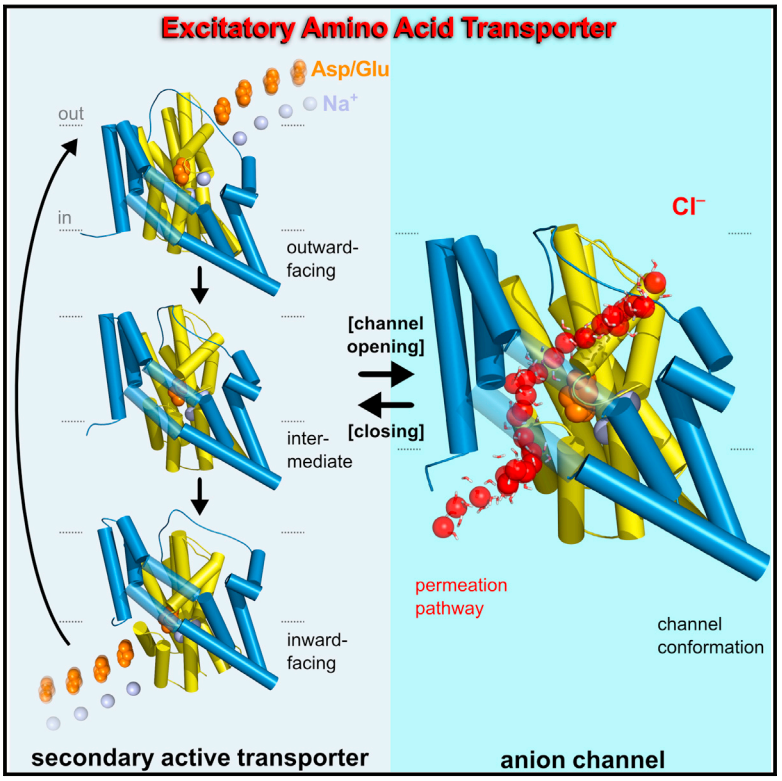

Highlights

- Molecular dynamics simulations define anion-conducting transporter conformations
- Anion permeation occurs along a well-defined, conserved permeation pathway
- Transport intermediates open the channel via steric and hydrophobic gating
- Anion selectivity is achieved via a single, structurally conserved arginine

Authors

Jan-Philipp Machtens, Daniel Kortzak, ..., Rodolfo Briones, Christoph Fahlke

Correspondence

jan-philipp.machtens@gmx.de (J.-P.M.), c.fahlke@fz-juelich.de (Ch.F.)

In Brief

Excitatory amino acid transporters operate both as transporters and as anion-selective ion channels at synapses. A combination of simulations and experiments with prokaryotic and mammalian glutamate transporter homologs defines the anion conduction pathway and elucidates how a class of secondary active transporters can function as perfectly selective, gated anion channels.

Machtens et al., 2015, Cell *160*, 542–553
January 29, 2015
http://dx.doi.org/10.1016/j.cell.2014.12.035

CellPress

Cell

Article

Mechanisms of Anion Conduction by Coupled Glutamate Transporters

Jan-Philipp Machtens,[1,2,3,*] Daniel Kortzak,[1] Christine Lansche,[1] Ariane Leinenweber,[2] Petra Kilian,[2] Birgit Begemann,[2] Ulrich Zachariae,[4] David Ewers,[2] Bert L. de Groot,[3] Rodolfo Briones,[3] and Christoph Fahlke[1,*]

[1]Institute of Complex Systems, Zelluläre Biophysik (ICS-4), Forschungszentrum Jülich, 52428 Jülich, Germany

[2]Institut für Neurophysiologie, Medizinische Hochschule Hannover, 30625 Hannover, Germany

[3]Computational Biomolecular Dynamics Group, Max Planck Institute for Biophysical Chemistry, 37077 Göttingen, Germany

[4]School of Engineering, Physics, and Mathematics and Division of Computational Biology, College of Life Sciences, University of Dundee, Dundee DD1 5EH, UK

*Correspondence: jan-philipp.machtens@gmx.de (J.-P.M.), c.fahlke@fz-juelich.de (Ch.F.)

http://dx.doi.org/10.1016/j.cell.2014.12.035

SUMMARY

Excitatory amino acid transporters (EAATs) are essential for terminating glutamatergic synaptic transmission. They are not only coupled glutamate/Na^+/H^+/K^+ transporters but also function as anion-selective channels. EAAT anion channels regulate neuronal excitability, and gain-of-function mutations in these proteins result in ataxia and epilepsy. We have combined molecular dynamics simulations with fluorescence spectroscopy of the prokaryotic homolog Glt_{Ph} and patch-clamp recordings of mammalian EAATs to determine how these transporters conduct anions. Whereas outward- and inward-facing Glt_{Ph} conformations are nonconductive, lateral movement of the glutamate transport domain from intermediate transporter conformations results in formation of an anion-selective conduction pathway. Fluorescence quenching of inserted tryptophan residues indicated the entry of anions into this pathway, and mutations of homologous pore-forming residues had analogous effects on Glt_{Ph} simulations and EAAT2/EAAT4 measurements of single-channel currents and anion/cation selectivities. These findings provide a mechanistic framework of how neurotransmitter transporters can operate as anion-selective and ligand-gated ion channels.

INTRODUCTION

Secondary active glutamate transport by excitatory amino acid transporters (EAATs) (Kanner and Sharon, 1978) terminates glutamatergic synaptic transmission and regulates glutamate concentrations within the CNS. EAATs can also function as anion-selective channels (Fairman et al., 1995; Wadiche and Kavanaugh, 1998), with EAAT anion channels regulating cell excitability and synaptic transmission (Picaud et al., 1995). Their physiological relevance is emphasized by the recent discovery that altered EAAT anion conduction is associated with episodic ataxia and epilepsy (Winter et al., 2012).

EAAT anion permeation occurs through a defined anion-selective conduction pathway (Kovermann et al., 2010), which is opened and closed through conformational changes coupled to transitions within the glutamate uptake cycle (Bergles et al., 2002; Machtens et al., 2011a; Otis and Kavanaugh, 2000). The channels are perfectly anion selective (Wadiche and Kavanaugh, 1998) and exhibit unitary current amplitudes, which are small but of a similar size range to those of specialized anion channels (Schneider et al., 2014). The five mammalian EAATs differ in their relative glutamate transport rates and anion currents, resulting in isoform-specific differentiation into efficient transporters associated with small macroscopic anion currents and low-capacity transporters that predominantly conduct anions (Mim et al., 2005). However, the functional properties of the underlying anion channels are very similar for each type (Schneider et al., 2014; Torres-Salazar and Fahlke, 2007), indicating conservation of the anion-conducting pore among functionally specialized transporters. So far, the localization of this conduction pathway, the underlying conformation of the transporter, and the mechanisms of anion permeation have not been identified.

We used molecular dynamics (MD) simulations to identify which conformations of the archeal glutamate transporter homolog Glt_{Ph} (Yernool et al., 2004) permit anion permeation and to characterize the molecular features of anion conduction. We analyzed the conformational changes leading to the formation of an anion-selective pore and observed ion permeation along this path in simulations. Using mutagenesis, fluorescence spectroscopy experiments on Glt_{Ph} and patch-clamp recordings on mammalian EAATs, we confirmed that the anion channel conformation we identified exists under experimental conditions and that this permeation pathway is utilized by both prokaryotic and mammalian glutamate transporters.

RESULTS

Molecular Dynamics Simulations Identify Anion-Conducting Conformations of Glt_{Ph}

Glt_{Ph} shares about 37% sequence identity with mammalian EAATs and is an accepted model of this class of transporters for studying secondary active transport and anion conduction (Boudker et al., 2007; Groeneveld and Slotboom, 2010; Ryan and Mindell, 2007; Yernool et al., 2004). High-resolution crystal

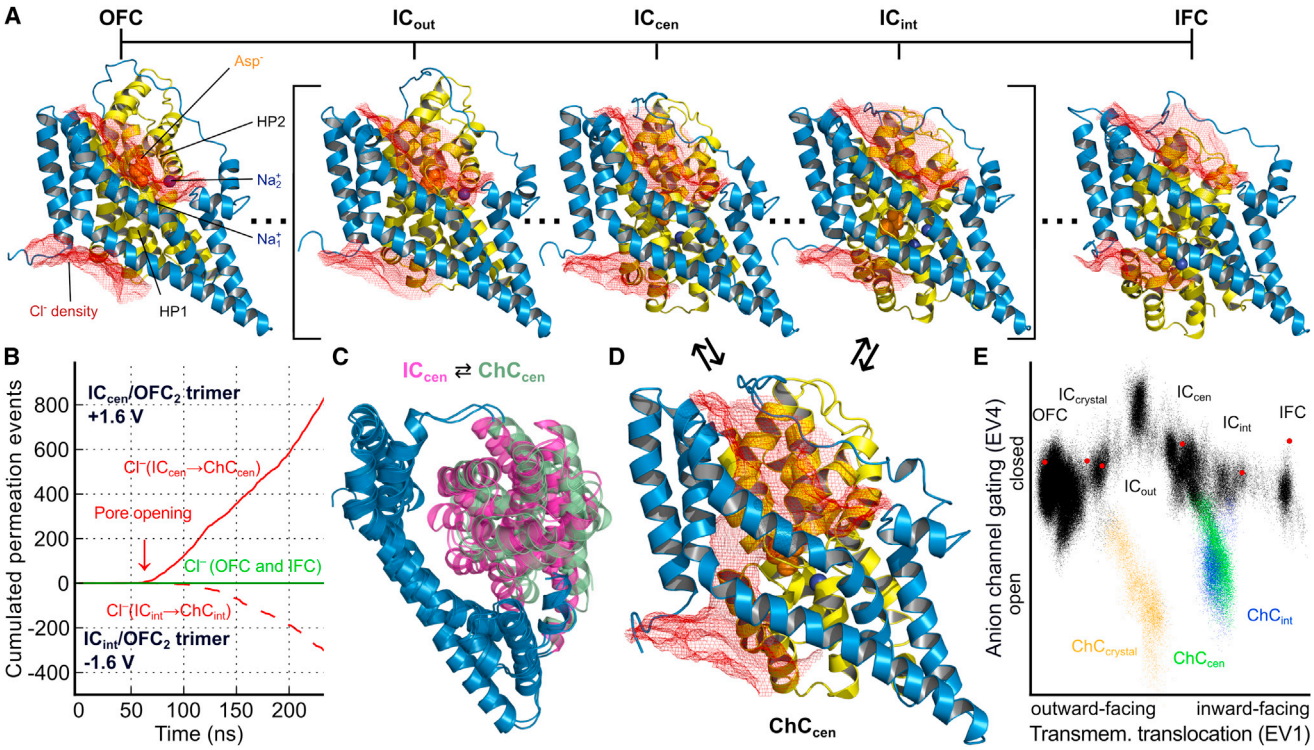

Figure 1. An Anion-Selective Conduction Pathway Is Formed by a Substrate Transport Intermediate

(A) Red isodensity meshes illustrate the Cl^- distribution (0.2σ) in MD simulations at +1.6 V around substrate-bound Glt_{Ph} monomers in various conformations (trimerization domain shown in blue; transport domain shown in yellow). The other two monomers, water molecules, lipids, and ions were omitted for clarity. Nonconductive outward-facing (OFC), inward-facing (IFC), and intermediate conformations (ICs; derived using essential dynamics sampling of the transition from OFC to IFC) are shown in side view.

(B and C) Ion permeation (B) and conformational change (C) of IC_{cen} during transition to an open channel conformation (overlay of IC_{cen} and ChC_{cen}, top view) upon application of a membrane potential (±1.6 V).

(D) Transitions of ICs into open channel conformations (ChCs) containing an anion-selective pathway occur at positive and negative potentials.

(E) Visualization of all trajectories (the OFC–IFC translocation/essential dynamics sampling simulation and separate MD simulations of OFC, IC_{out}, $IC_{crystal}$, IC_{cen}, IC_{int}, IFC, and of the ChCs of the intermediates) in the principal component space by projection onto the first (EV1) and fourth (EV4) eigenvectors, corresponding to translocation and pore formation, respectively. Black dots represent nonconducting conformations. Blue, green, and orange dots denote frames in MD trajectories, where Cl^- permeation through the respective ChC conformation was observed. Note that the point density is biased by the number and length of simulations initiated from the various starting conformations (red circles) and therefore does not provide information on energetics.

See also Figures S1, S2, and S3 and Movie S1.

structures revealed a trimeric assembly, with each subunit containing eight transmembrane helices (TM) and two hairpin loops (HP) (Yernool et al., 2004). Analysis of different conformations demonstrated that substrate translocation involves a large-scale (~18 Å) rotational translational movement of the substrate-harboring transport domain relative to the static trimerization domain (Crisman et al., 2009; Reyes et al., 2009).

We used all-atom MD simulations capable of directly simulating ion flux driven by transmembrane voltages (Kutzner et al., 2011) to investigate anion permeation in substrate-bound Glt_{Ph}. Simulations were performed using various Glt_{Ph} conformations in the presence of 1 M NaCl on either side of the membrane. Positive and negative membrane potentials (initially ±1.6 V; later ±800 mV) applied to increase anion permeation rates had no detrimental effects on the stability of the system (Figure S1 available online), in good agreement with the results of other simulation studies (Jensen et al., 2012). Within a total simulation time of >8 μs, no Cl^- permeation events were observed for the known outward- (OFC) and inward-facing (IFC) conformations at membrane potentials up to ±1.6 V, indicating that none of these states is anion conducting (Figures 1A and 1B; Extended Experimental Procedures). We concluded that translocation intermediates might correspond to the precursors of anion-conducting conformational states and simulated the OFC–IFC transition to obtain novel intermediate conformations (ICs) using essential dynamics sampling (Amadei et al., 1996). In these simulations, the transporter was driven along the first eigenvector (EV1)—representing transmembrane translocation of the transport domain—from a principal component analysis (PCA) of the conformational changes of transporter monomers in simulations on OFC and IFC (Figures 1A, S1C, and S1D). Because individual subunits function independently within the trimeric assembly (Erkens et al., 2013; Grewer et al., 2005), translocation simulations were performed on a single monomer—with the other two remaining in the OFC. These simulations correctly sampled the recently crystallized Glt_{Ph} intermediate ($IC_{crystal}$, minimum

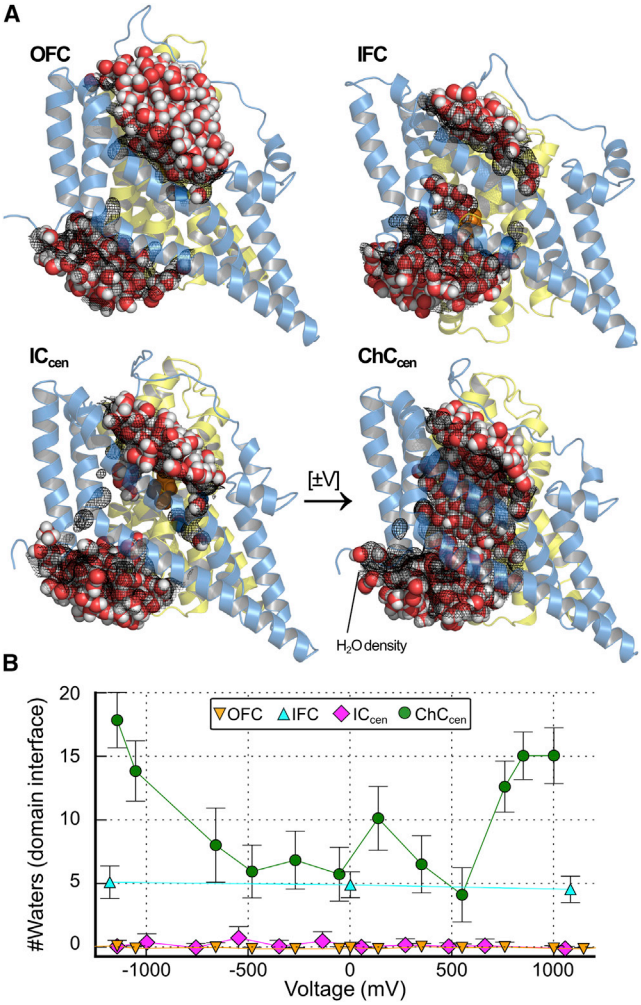

Figure 2. Hydrophobic Gating of the Anion Permeation Pathway

(A) Representative (spheres) and averaged (black mesh) water distribution in the transport/trimerization domain interface of Glt_{Ph} in various conformations (side view).

(B) Voltage-dependent occupancy of the interface core region by water molecules (counted within a cylindrical slab; each data point corresponds to a 100 ns simulation). Note that increased water numbers in ChC, but not in IFC, result in the formation of a continuous water bridge between the extra- and intracellular space (A). Error bars indicate the SD of the water molecule counts during the simulations.

monomeric root-mean-square deviation [RMSD] of 1.3 Å). This demonstrates the existence and stability of translocation intermediates (Verdon and Boudker, 2012) and validates the simulated transition pathway (Figure S2C). We then chose three intermediates, IC_{out} (similar to $IC_{crystal}$), IC_{cen}, and IC_{int}, from our trajectory that were equally distributed between the OFC and IFC, and, together with $IC_{crystal}$, subjected them to further MD under transmembrane voltage (Figures 1A and S1).

All intermediates were impermeable to Cl^- and remained closed for hundreds of nanoseconds in the absence of membrane voltage (Figures 1A and S1G; Extended Experimental Procedures). However, for $IC_{crystal}$, IC_{cen}, and IC_{int}, lateral movement of the transport domain occurred 70–300 ns after applying membrane potentials $\geq \pm 1.3$ V. These conformational changes resulted in open channel conformations (designated here as $ChC_{crystal}$, ChC_{cen}, or ChC_{int}) that were centrally localized on the translocation reaction coordinate and that exhibited an anion-selective conduction pathway at the interface between the trimerization and transport domains, near the tip of HP1 (Figures 1B–1D; Movie S1). Pore opening and closing always reversed after changing the applied voltage, and neither protein instability nor electroporation through the lipid bilayer were observed (Figures S1E–S1H and S3A–S3E). Pore opening occurred from various intermediate conformations, however, with different opening propensities in the order of $IC_{out} < IC_{crystal} < < IC_{int} < IC_{cen}$. For IC_{out} and $IC_{crystal}$, channel opening was never or only once observed (0 out of 4 [IC_{out}] or 1 out of 5 [$IC_{crystal}$, at +1.6 V] simulations) within ~400 ns for each (Figures S2D and S2E). In contrast, such transitions were regularly seen for IC_{cen} and IC_{int} (20 out of 20 [IC_{cen}, at 1.3–1.6 V] or 4 out of 4 [IC_{int}, −1.6 V] simulations) (Figure 1B). To further analyze the conformational changes underlying channel opening and to relate them with translocation of Glt_{Ph}, we performed an additional PCA on all data, including the previously used set of OFC and IFC trajectories, the translocation simulations and all simulations of intermediates under membrane voltages. In addition to EV1—which remained unchanged compared with the first PCA and represents translocation—we found that conformational changes along the fourth eigenvector (EV4) correlated with the onset and ending of anion permeation (Figures S3C–S3E). We plotted the position taken up by the trajectories in the principal component space, as defined by eigenvectors EV1 and EV4, which describe conformational changes attributed to translocation and anion channel gating, respectively (Figure 1E). Although originating from different intermediate states, open channel conformations ChC_{cen} and ChC_{int} had RMSDs approaching 1.0 Å with similar overall structures and will be treated as a single conformation (ChC) (Figures 1E and S3F–S3H).

Formation of the anion conduction pore at the interface between the transport and trimerization domains is accompanied by extensive hydration of this region and the creation of a continuous water bridge spanning the membrane (Figure 2A). In each of our simulations, this process was reversible with channel closure preceded by complete dewetting. Water entry is promoted by both positive and negative potentials with voltage-independent water occupancy between −400 and +400 mV (Figure 2B). The hydrophobic environment of this region (see below) is expected to represent a barrier to anion permeation that can be dynamically lowered by the entry of water molecules. Wetting of the rather hydrophobic interface region might compensate for the energetic cost of breaking hydrophobic interactions between the surfaces of the trimerization and transport domains during the conformational change that broadens the interface. Therefore, we suggest that channel opening and closing is mediated by a combination of steric and hydrophobic gating, as has been demonstrated for some other ion channels (Jensen et al., 2012; Vaitheeswaran et al., 2004).

Structural Determinants of Glt_{Ph} Anion Permeation

The Glt_{Ph} anion conduction pathway has a distorted hourglass shape, with large extra- and intracellular entrance cavities that

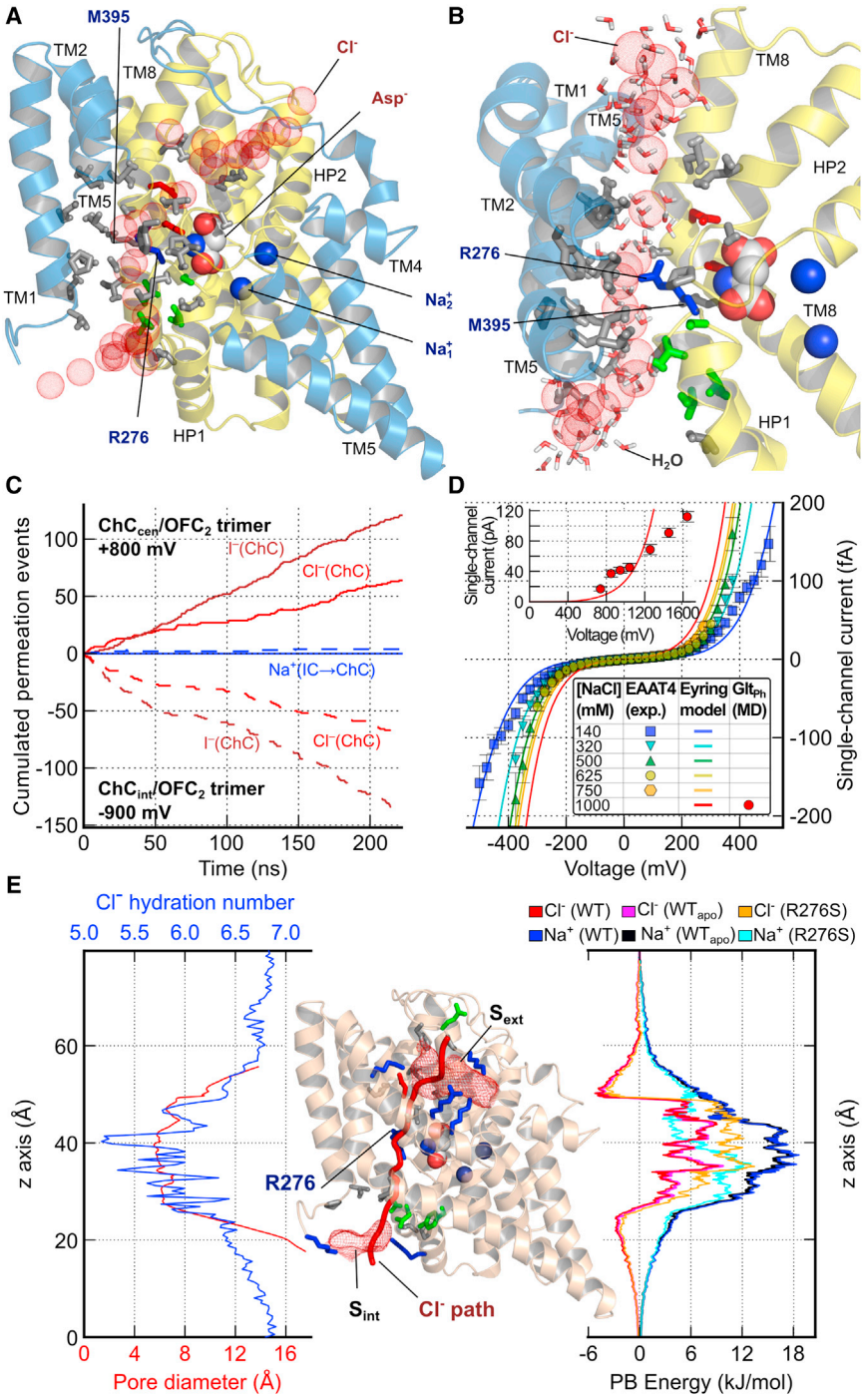

Figure 3. Structural Determinants of Glt_{Ph} Anion Permeation

(A) Cartoon representation of a ChC_{cen} monomer (light blue, trimerization domain; yellow, transport domain) in side view from the subunit interface, with pore-lining side chains shown as sticks (blue, positive; red, negative; green, polar; gray, apolar). TM2 and TM5 are partially omitted for clarity. Red spheres represent snapshots of a single permeating Cl^- ion.

(B) Close-up of the permeation pathway from the TM4–TM5 loop. Coloring as in (A), including representative water molecules found in the inner hydration shell of permeating Cl^- ions.

(C) Count of Cl^- and I^- permeation events through ChC_{cen} and ChC_{int} at +800 and −900 mV (dashed lines), respectively.

(D) EAAT4 current voltage plots for various symmetrical [NaCl]. Single-channel currents were determined by multiplying whole-cell Cl^- currents recorded 1 ms after the voltage jump (means ± SE, n > 10 for each condition) by the ratio of experimentally measured unitary current (Figure 6B) and mean current amplitudes (n = 12) at +150 mV in 140 mM NO_3^-. The experimental data (symbols) were globally fitted using a three-binding site Eyring rate model (lines; Extended Experimental Procedures). The inset displays Glt_{Ph} unitary current amplitudes (red symbols) from MD simulations using 1 M NaCl and the extrapolation of the experimental data to these conditions by the Eyring model (red line).

(E) Pore profile of anion hydration, pore diameter, and Poisson-Boltzmann energies for Na^+ and Cl^- of WT and R276S and of WT Glt_{Ph} in an apo state, i.e., after removal of aspartate and Na^+ ions (in ChC_{cen}). Hydration numbers are the average number of hydrogens within the first Cl^- hydration shell. Cl^- isodensity meshes around ChC_{cen} (4.2σ) illustrate two Cl^--binding sites at the channel entrances, denoted S_{ext} and S_{int}.

See also Figure S4.

narrow to a more constricted conduction path almost perpendicular to the membrane (Figures 1D, 3A, and 3B; Movie S1). Pore-forming residues are highly conserved between Glt_{Ph} and mammalian EAATs (Figure S4). This level of conservation is consistent with the functional similarity between Glt_{Ph} (Ryan and Mindell, 2007) and EAAT anion channels (Melzer et al., 2003; Wadiche and Kavanaugh, 1998) and accounts for similar unitary current amplitudes among EAATs with large glutamate transport and small anion current components and those with predominant anion conductance (Schneider et al., 2014; Torres-Salazar and Fahlke, 2007). Most side chains lining the pore center are hydrophobic, except for R276, which protrudes from the tip of HP1 into the Cl^- density (Figures 3A and 3B). EAATs lack a positive side chain at the position corresponding to R276, but contain arginine at positions homologous to M395 of Glt_{Ph} (Ryan et al., 2010) (Figure S4). MD simulations of the R276S-M395R Glt_{Ph} mutant (see below) showed that both the arginine in the "EAAT position" and R276 project their side chain toward the same location, resulting in conservation of the positive charge at this site in the tertiary structure of EAATs and Glt_{Ph} (Figures 3A and 3B).

Starting from the ChC_{cen} conformation, we simulated anion permeation at reduced voltages of ±~800 mV and observed

perfect anion selectivity (Figure 3C). In 1 M NaCl, our simulations yielded single-channel anion currents of 42.4 ± 6.3 pA (∼+800 mV) or 51.4 ± 6.7 pA (∼−900 mV). These voltages and salt concentration are too high to permit direct experimental verification of the conductances. We measured EAAT4 anion currents at 140–750 mM NaCl and at voltages up to 500 mV (Figure 3D) to extrapolate the voltage dependence of EAAT4 unitary anion currents to the MD conditions. Comparing these experimental EAAT4 and simulated Glt_{Ph} current-voltage relationships demonstrated that simulations reproduce the experimental unitary current amplitudes within the same order of magnitude (Figure 3D, inset). Substitution of Cl^- by I^- in the simulations resulted in significantly higher anion currents of 95.0 ± 5.4 pA (∼+800 mV) or of 97.1 ± 10 pA (∼−900 mV; Figure 3C); however, the transport substrate aspartate did not permeate within 200 ns at concentrations of ∼500 mM. Simulated permeation properties thus closely resemble the functional characteristics of mammalian EAATs (Melzer et al., 2003; Wadiche and Kavanaugh, 1998).

The electrostatic Poisson-Boltzmann energy profile for moving an ion along the channel axis displays much higher energy barriers for Na^+ than for Cl^- (Figure 3E). Energy wells at both entrances with high Cl^- densities represent Cl^- binding sites, denoted S_{ext} and S_{int}. The critical role of R276 in anion selectivity is demonstrated by the convergence of Na^+ and Cl^- energy barriers upon removal of the positive charge in R276S Glt_{Ph} (Figure 3E). Energy profiles are identical in both the presence and absence of bound aspartate/Na^+ at their binding sites (Figure 3E). Simulated ion permeation through this apo state revealed similar Cl^- permeation rates along the same permeation pathway (data not shown), consistent with the experimentally determined unitary conductances of EAATs being indistinguishable in the presence and absence of substrate (Kovermann et al., 2010). The conduction pathway is rather wide with a minimum diameter of 5.6 Å, such that anions can permeate in a partially hydrated state, and Cl^--H_{water} coordination numbers show only a small decrease from 6.8 in bulk solution to 5.2 in the Glt_{Ph} channel center (Figure 3E).

Tryptophan-Scanning Mutagenesis Reveals Direct Interactions of Predicted Pore-Forming Residues with Permeant Anions

We used a combination of tryptophan-scanning mutagenesis and iodide quenching (Vázquez-Ibar et al., 2004) to test whether permeating anions come into close contact with amino acid side chains projecting into the proposed anion conduction pathway. I^- readily permeates through Glt_{Ph} and EAAT anion channels and is therefore expected to come into close proximity to residues forming the permeation pathway. Because I^- can reduce tryptophan fluorescence via direct interactions, i.e., collisional quenching (Lakowicz, 2006), iodide quenching of tryptophan fluorescence is a suitable method to experimentally verify the simulated Glt_{Ph} anion permeation pathway. As Glt_{Ph} lacks endogenous tryptophans, we generated single-tryptophan mutants by substituting 13 residues that protrude from the trimerization domain into the interface region of Glt_{Ph} ChC_{cen} (Figure 4A). To avoid interference with substrate binding, we did not insert tryptophan residues into the transport domain. With the exception of S65W, I^- reduced fluorescence in all Glt_{Ph} mutants in a concentration-dependent manner. Figure 4B shows the spectral properties of V51W and S65W Glt_{Ph} in detergent micelles and their modification at various [I^-]. The identical concentration dependences of the fluorescence lifetimes and intensities indicate that I^- quenches tryptophan fluorescence via a collisional mechanism (Figure 4B, inset).

Figure 4A maps the relative quenching (F_o/F) at [I^-] = 350 mM of the tested tryptophan residues on the ChC_{cen} structure. These data demonstrate the high iodide accessibility of residues close to the proposed anion permeation pathway, which is reduced with increasing distance. Linear concentration dependences of F_0/F in Stern-Volmer plots are expected for proteins with a single tryptophan, which adopt only one conformation. The observed deviations from linearity indicate that tryptophan-substituted Glt_{Ph} mutants assume multiple conformations that differ in I^- accessibility (Figure 4C). These findings support the notion that tryptophan-substituted Glt_{Ph} mutants exhibit similar degrees of conformational heterogeneity to wild-type (WT) Glt_{Ph}.

Figure 4D shows plots of the calculated anion accessibilities in simulations of different conformations compared with experimentally observed fluorescence quenching. Most residues are accessible in multiple conformations. However, there are three residues—W50, W54 (projecting directly into the anion pore), and W62 (at a more peripheral location)—with rather exclusive anion accessibility in ChC (Figures 4D and S5; see the Extended Experimental Procedures for details on the calculation of anion accessibilities from the simulations). For these constructs, a modified Stern-Volmer analysis was used to determine the fraction of fluorescence quenchable by I^- to be ∼20% (Figures S5A and S5B). Because different protein conformations could exhibit different quantum yields of the inserted tryptophan, this value is not always identical to the probability of the protein assuming this accessible conformation. However, these data indicate that Glt_{Ph} can assume the anion-conducting channel conformation ChC even in the absence of an applied voltage and that this conformation is sufficiently stable to permit I^- collisions with side chains that project into the anion conduction pathway.

Mutations of Pore-Forming Residues Affect Unitary Anion Current Amplitudes and Anion/Cation Permeability Ratios

To provide further verification of the predicted anion permeation pathway, we compared the effects of amino acid exchanges on simulated and experimental permeation properties. We chose experimental measures corresponding to parameters obtained from MD simulations: these included the single-channel conductance and the anion/cation selectivity of the anion channel. In contrast, macroscopic current amplitudes alone, e.g., from whole-cell recordings, do not permit a distinction to be made between mutations that alter the anion permeation rate or those that affect the probability of assuming an open anion channel state and therefore preclude a direct comparison with simulation results. Because of difficulties in cellular expression systems, high-resolution electrophysiological recordings of Glt_{Ph} are not yet feasible. Assays that were developed to describe Glt_{Ph} anion conductance (Ryan and Mindell, 2007) only provide information

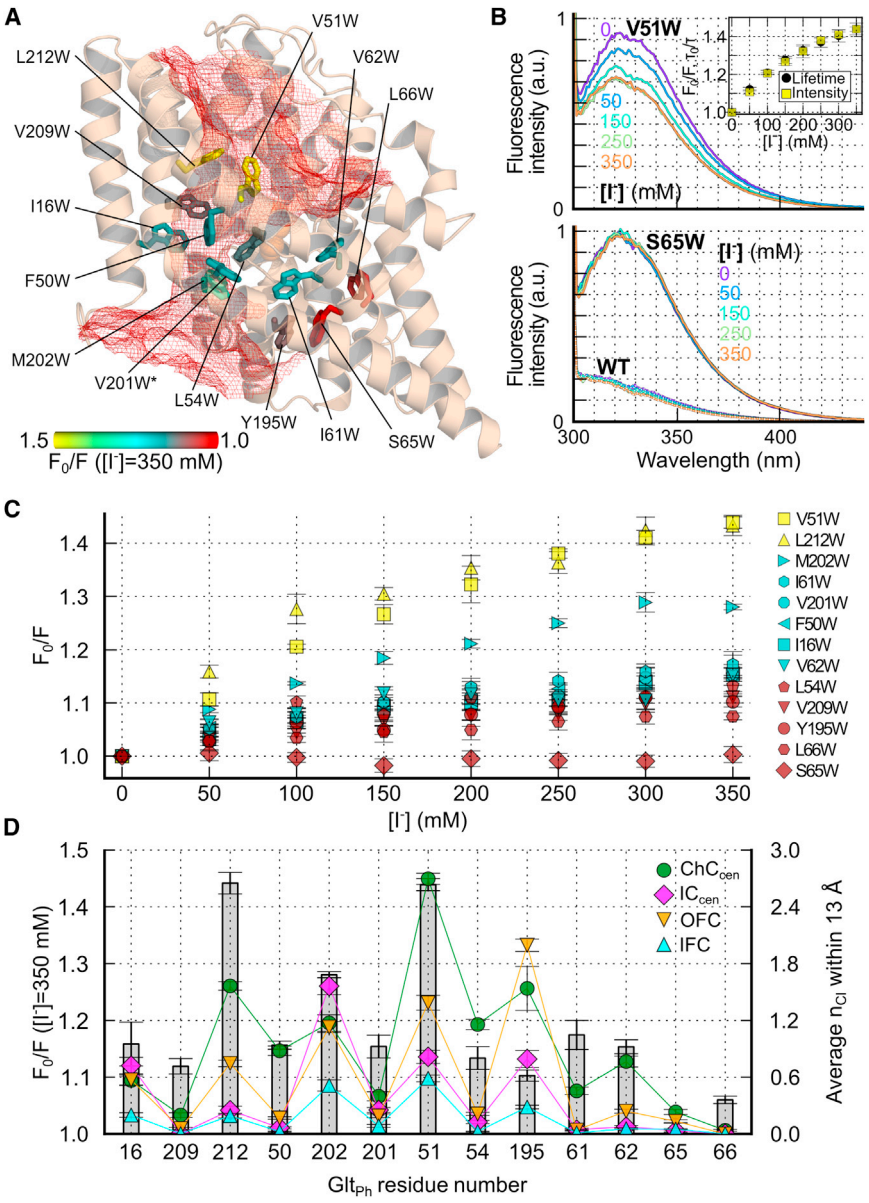

Figure 4. Tryptophan Fluorescence Quenching by Iodide in Glt_{Ph}

(A) Overview of Glt_{Ph} single-tryptophan insertions (ChC_{cen} in side view). Side chains are color-coded according to the reduction in fluorescence intensity at 350 mM [I^-] (F_0 is the intensity in the absence of I^-; n ≥ 5 for each). Red mesh represents the Cl^- density observed in MD (Figure 1D).

(B) Representative fluorescence spectra of WT, V51W, and S65W Glt_{Ph} at various [I^-]. The inset shows the comparable concentration dependence of V51W fluorescence lifetimes and intensities in a Stern-Volmer plot, indicating a collisional quenching mechanism.

(C) Stern-Volmer plots for all tryptophan mutants (means ± SE; n ≥ 5 for each).

(D) Comparison of fluorescence quenching (gray bars; n ≥ 5 for each) with MD-predicted anion accessibilities of side chains in various conformations (the different symbols show the average number of Cl^- ions ± SD within 13 Å of the side chains). Residue numbers on the abscissa are ordered according to their positions in the membrane plane shown in (A).

See also Figure S5.

We initially screened for mutations that affect pore properties in silico. Pore-forming residues were identified by a geometrical criterion (within a distance <6.9 Å to the pore center defined by R276). We excluded only a few residues that are located within the transport domain and known to be crucial for substrate binding (e.g., residues in HP2 to prevent interference with substrate binding). We generated 29 Glt_{Ph} pore mutants in silico, including S65 and I61, which are close to a recently discussed alternative location of the anion channel (see below) and subjected them to MD simulations. We identified side-chain substitutions that increase or decrease unitary conductances (I16E/K, L20E, F50L/K/D, V51D, L54D, I61D, A205D, R276S/D) or modify the anion/cation selectivity (F50D, A205D, R276S) (Figure 5). We then performed whole-cell patch-clamp recordings of 33 EAAT2/EAAT4 mutants (Figure S6). Because most mutations also affected anion channel gating (Figure S6), a direct comparison of whole-cell currents and MD data was not feasible. However, ten EAAT4 mutants exhibited sufficient time- and voltage-dependent gating to allow single-channel conductances to be determined using nonstationary noise analysis (Figure 6). Four charge-altering mutations, L20E, I16K, I16E and I61D, increased or decreased the simulated Cl^- permeation rate of Glt_{Ph} to a similar extent as alterations in experimental single-channel conductance caused by the homologous EAAT4 mutations. For four Glt_{Ph} mutants, V12E, I16W, and S65A, experimental and simulated unitary conductances were unaltered (Figure 6B). Interestingly, I16E—located in the intracellular part of the

about macroscopic anion currents through an ensemble of multiple Glt_{Ph} transporters. Because the functional properties of Glt_{Ph} (Ryan and Mindell, 2007) and EAAT anion channels are very similar (Melzer et al., 2003; Wadiche and Kavanaugh, 1998) and the pore-lining residues are highly conserved (Figure S4), it is reasonable to assume that the proposed Glt_{Ph} anion permeation pathway is also responsible for EAAT anion conduction. We therefore compared the effects of in silico mutagenesis on simulated Glt_{Ph} anion conductance and anion/cation selectivity with experimental data on mammalian EAAT2/EAAT4. Single-channel recordings have not yet been possible for these transporters, but unitary current amplitudes can be determined by noise analysis of whole-cell current recordings, and anion/cation selectivities can be obtained through reversal potential measurements at various ionic conditions (Melzer et al., 2003).

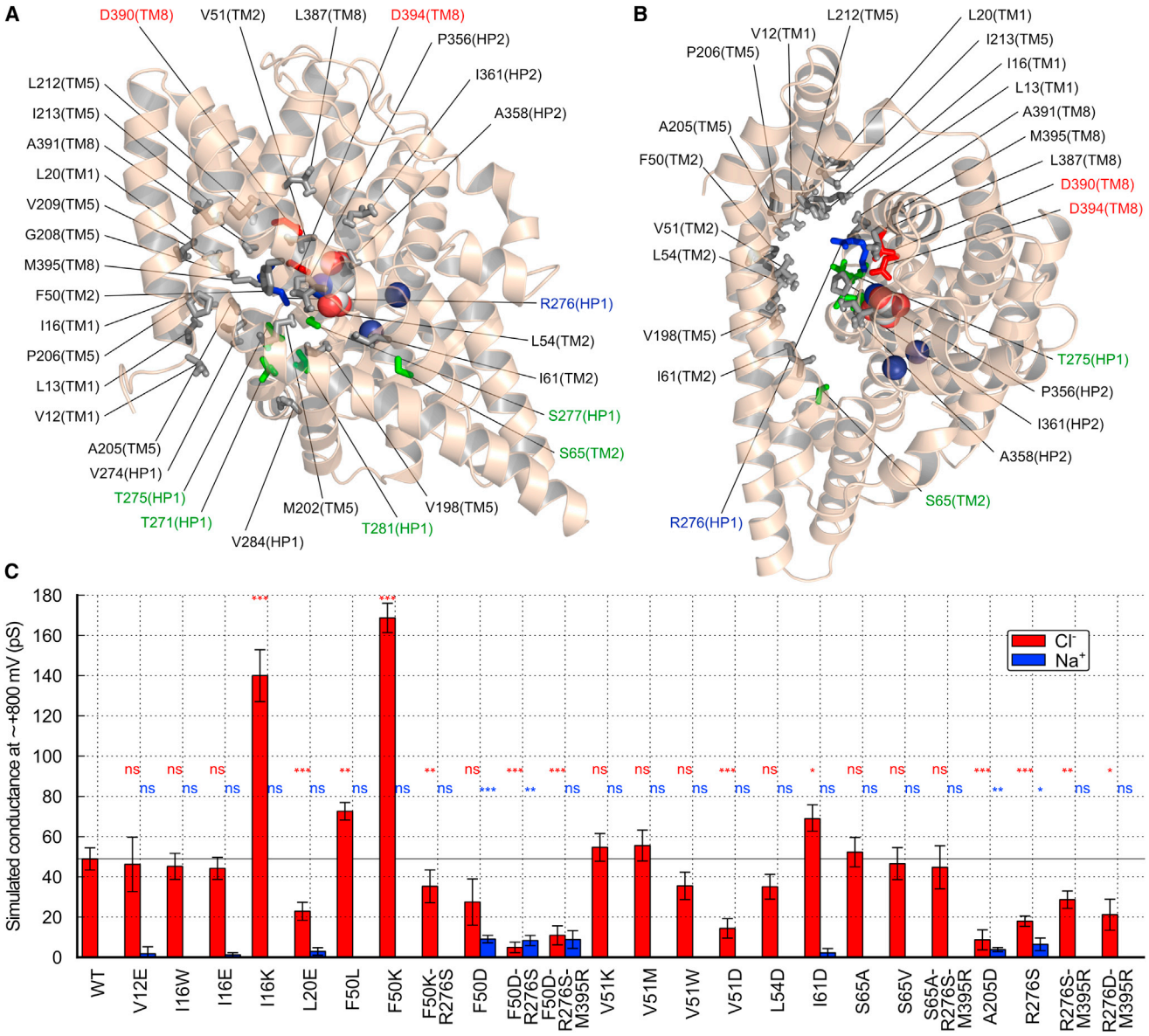

Figure 5. MD Screening of Pore-Lining Residues Predicts Mutations that Affect Anion Conductance and Anion/Cation Selectivity

(A and B) Stick representations of pore-lining residues in side view (A) or top view (B) and colored as in Figure 3A, including detailed Glt_{Ph} residue number labels. (C) Summary of simulated Na^+/Cl^- conductances for various Glt_{Ph} mutants (ChC_{cen}; means ± SD; MD times range from 120 to 500 ns for each mutant) at ~+800 mV.

Glt_{Ph} anion conduction pathway—selectively reduced outward fluxes of anions in a valve-like manner, as demonstrated by outward current rectification in the I16E Glt_{Ph} and homologous T59E EAAT4 mutants. In contrast, for the neighboring residue V12, which is closer to the bulk solution and further from the pore center than I16 (Figure 5A), conversion to glutamate did not affect unitary conductances in Glt_{Ph} or in F55E EAAT4. We furthermore found four "semiconserved" side chains that are conserved within mammalian EAATs but differ in Glt_{Ph}: the aforementioned R276 residue (the corresponding EAAT arginine is located at the M395 position in Glt_{Ph}), F50 (L in EAATs), and M94 (V in EAATs; Figure S4). We constructed Glt_{Ph} and EAAT4 mutants to reverse these evolutionary exchanges and observed reciprocal effects on conductance, as would be expected if direct interactions exist between these side chains and permeating anions (Figure 6C).

The simulated Glt_{Ph} mutants F50D, A205D, and R276S exhibited Na^+ permeation along the same path as Cl^- (Figures 7A and 7C). Because some of the corresponding EAAT4 mutations prevented their functional expression in cells, homologous mutations were introduced into EAAT2, a transporter with unitary current properties similar to those of EAAT4 (Schneider et al., 2014).

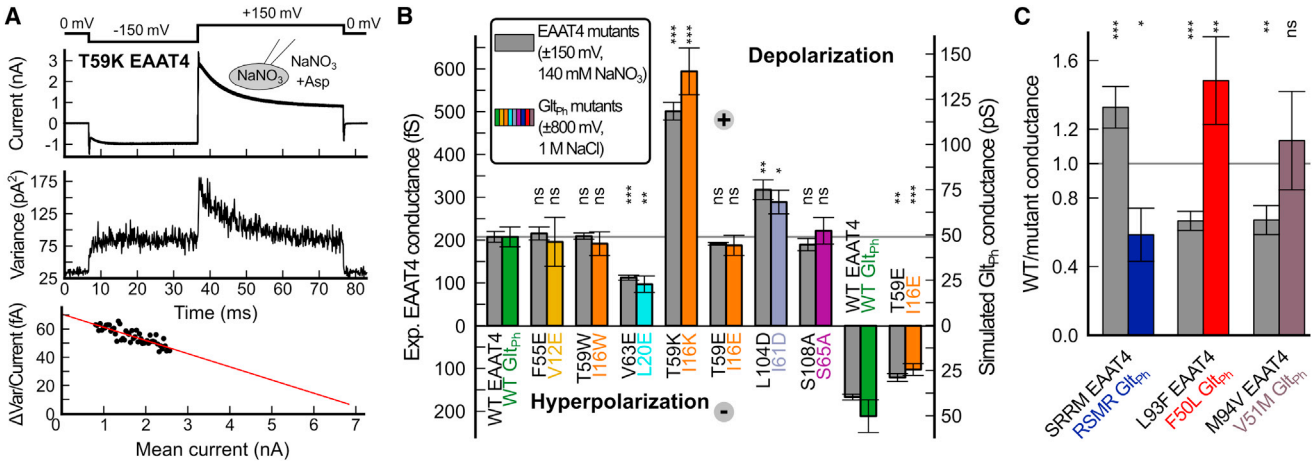

Figure 6. Mutations of Pore-Forming Residues Modify Experimental EAAT4 Anion Conductances and Anion/Cation Selectivity

(A) Representative nonstationary noise analysis of T59K EAAT4, showing current responses to 300 repeated voltage jumps (top) and the resulting current variances (middle). Bottom, linearly transformed current-variance plot (background noise at 0 mV was subtracted from the total variance). Red line shows a linear fit.

(B) Experimental EAAT4 (gray; from whole-cell recordings and nonstationary noise analysis; means ± SE; n = 6–9) and simulated Glt_{Ph} unitary conductances of WT and homologous mutants (in color; means ± SD). Ordinates were scaled to show experimental WT EAAT4 conductances at +150 mV and simulated WT Glt_{Ph} conductances at +800 mV at the same level (gray line).

(C) Changes in experimental EAAT4 (n = 6–8) and simulated Glt_{Ph} unitary conductance upon substitution of residues that are conserved in EAATs, but not in Glt_{Ph} (Figure S4).

See also Figures S6 and S7 and Table S1.

Varying the external [Na^+] led to changes in ion current reversal potentials in cells expressing L85D, S288D, and R476M EAAT2, indicating that EAAT2 mutants represent unselective channels with varying degrees of relative cation selectivity (Figure 7B). In these experiments, coupled glutamate transport, which would additionally affect the reversal potential, was abolished by using a K^+-free intracellular solution.

The effect of these negative charge mutations was site-specific as demonstrated by experiments and simulations with A362D EAAT2 and the corresponding R276D-M395R Glt_{Ph}. A362 in EAAT2 is homologous to R276 in Glt_{Ph}, whose positively charged side chain is crucial for anion selectivity (Figure 3). To achieve the electrostatic potential in Glt_{Ph} to be similarly modified as in A362 EAAT2, we inserted an arginine at the "EAAT position" M395, in addition to the R276D mutation (Figures 3A and S4). R276D-M395R Glt_{Ph} and A362D EAAT2 exhibited perfect Cl^- selectivity in both simulations and experiments, indicating that anion selectivity is only impaired by the insertion of negatively charged side chains at specific positions (Figures 5 and 7).

The Novel Anion Channel Conformation Enables a Reinterpretation of Previous Functional Data and Is Compatible with Published Crosslinking Results

Prior to our work, the structural basis of EAAT/Glt_{Ph} anion conduction was unknown. However, because mutations around S65 were reported to affect anion permeation of both Glt_{Ph} (Ryan and Mindell, 2007) and EAAT1 (Cater et al., 2014; Ryan et al., 2004), and because crystallographic data (Verdon and Boudker, 2012) suggested the existence of an aqueous cavity in $IC_{crystal}$, it has been hypothesized that anions permeate along a pathway that we will refer to as "S65 path" (Figure S7A). As yet, no other EAAT anion permeation pathway has been proposed.

We performed MD simulations and experimental approaches to test whether anion permeation along the "S65 path" might contribute to EAAT/Glt_{Ph} anion conduction. MD simulations demonstrated water access but no Cl^- density along the "S65 path" in ChC (Figure S7A). Pore searching algorithms (see the Extended Experimental Procedures) did not identify any additional candidate anion pore in the S65 region. Mutations of S65 did not affect anion conductance in MD simulations (Figure 5). In our fluorescence assay, S65W Glt_{Ph} fluorescence was not quenched by iodide (Figure 4). Whereas the homologous S108V EAAT4 mutant was mostly retained in intracellular compartments, S108A EAAT4 was robustly expressed on the surface of mammalian cells, with resulting current amplitudes comparable with those of WT EAAT4. S108A EAAT4 exhibited altered anion channel gating but unaltered unitary current amplitudes (Figures 6B and S6). These results indicate that mutations of S65/S108 do not affect the single-channel conductance itself but instead alter the channel open probability, i.e., the rates of reactions leading to the open anion channel.

We generated three additional EAAT4 mutants (V101D, L104D, and N297D) with negatively charged side chains projecting into the "S65 path." Mutant channels exhibited altered voltage- and glutamate-dependent gating but were still glutamate sensitive and cation impermeable (Figures S6B, S6C, S7A, and S7B). One mutation in this region, I61D Glt_{Ph}/L104D EAAT4, even increased anion permeation rates in both simulations and experiments (Figures 5 and 6B). Because this residue does not directly line the Cl^- permeation pathway, which remained unchanged upon I61D substitution, and because the introduction of a negative charge increases anion conductance, we deduce that this mutation indirectly affects the anion channel function. We conclude that the mutated amino acids surrounding

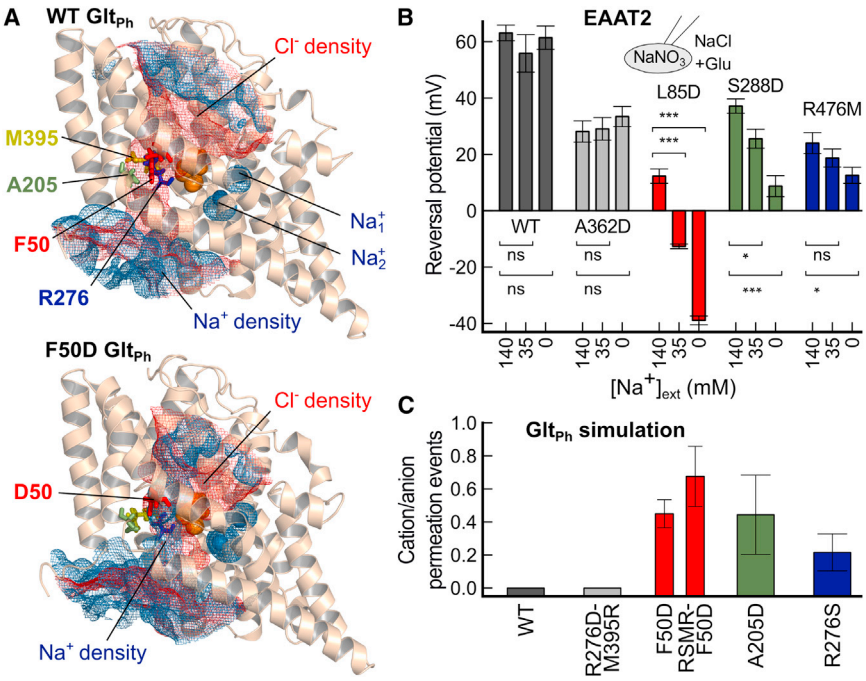

Figure 7. Conversion of the EAAT2 Anion Pore into a Cation-Conducting Channel

(A) Cl^- (red) and Na^+ (blue) distributions (σ = 0.2) around WT and F50D Glt_{Ph}. Residues described in (B) and (C) are shown as sticks.

(B) Variations in current reversal potentials with external [Na^+] demonstrate the cation permeability of L85D EAAT2—homologous to F50D Glt_{Ph}—S288D, and R476M (but not of WT and A362D) EAAT2 anion channels (means ± SE; n = 6–13 for each).

(C) Ratio of simulated cation/anion permeation events for WT and corresponding Glt_{Ph} mutants (means ± SD; RSMR, R276S-M395R), colored according to (B). The F50D mutant was tested with the arginine at position 276 (WT) and in the context of the EAAT arginine position (RSMR mutation).

See also Figures S6 and S7 and Table S1.

S65 in Glt_{Ph} do not line the EAAT anion pore, although they do influence the conformational changes underlying the probability of the channel being open.

A recent study demonstrated that crosslinking a substituted cysteine within the transport domain to another in the trimerization domain abolishes EAAT3 glutamate transport but does not abrogate substrate-dependent anion conductance (Shabaneh et al., 2014). The authors concluded that, starting from OFC, a limited inward movement of the transport domain is sufficient for formation of an anion conducting conformation. Cysteines were inserted at positions corresponding to residues 216 and 391 in Glt_{Ph}. These residues are in close proximity in OFC, IC_{out}, and $IC_{crystal}$. Because MD simulations demonstrated a pronounced increase in the V216–A391 C_α distance to >7 Å during transmembrane translocation and channel opening (Figure S7C), this disulfide link might prevent transitions into the IC_{cen}, IC_{int}, ChC, and IFC states. To evaluate the effects of this disulfide bridge on the conformational changes underlying anion channel opening, we performed simulations on an intermediate conformation of our translocation trajectory that is located at the most central position along the translocation axis (to increase the likelihood of pore opening) but maintains a distance between these two residues of $\leq$7 Å (Figures 1 and S7C). The crosslinkage was modeled by a distance restraint on the two C_α atoms within monomers (Figures S7C and S7D). Simulations of the V216–A391 crosslinked Glt_{Ph} model showed that this disulfide link limits the lateral movement of the transport domain but permits sufficient conformational flexibility for pore opening and anion permeation along the identified anion conduction pore (Figures S7E and S7F). The experimental effects of this crosslink on transport and anion currents in EAAT3 (Shabaneh et al., 2014) are therefore fully consistent with the Glt_{Ph} anion permeation pathway presented here.

DISCUSSION

EAAT glutamate transporters are prototypical dual function proteins that operate as both secondary active transporters and anion-selective ion channels. Whereas the key structural features of secondary active glutamate transport have been established (Akyuz et al., 2013; Crisman et al., 2009; Reyes et al., 2009; Shrivastava et al., 2008), structural and mechanistic details of anion permeation have been hitherto unknown. In this study, we used a combination of computational and experimental approaches to determine how this class of transporters mediates anion permeation through an aqueous conduction pathway. MD simulations identified an open channel conformation of Glt_{Ph} that was consistently formed from various ICs by the lateral movement of the transport domain (Figure 1). Opening of the interface between the transport and trimerization domains is followed by voltage-promoted water entry (Figure 2) and the formation of an anion-selective conduction pathway (Figure 3). We verified the predictions of our simulations by fluorescence spectroscopy and functional studies using mutant transporters. Fluorescence quenching experiments demonstrated that tryptophan residues substituted at positions that project into the predicted conduction pathway come into close contact with permeating anions (Figure 4). Moreover, substitution of pore-forming residues had comparable experimental effects on the two key characteristics of an anion-selective conduction pathway, i.e., anion/cation selectivity and ion permeation rates, as predicted by simulations (Figures 5, 6, and 7). These data indicate that pore-forming residues identified through simulations are indeed the major determinants of anion permeation and selectivity in both Glt_{Ph} and EAATs. Moreover, they demonstrate that this anion conduction pathway is conserved throughout the glutamate transporter family. Our data thus clarify how a class of secondary active transporters can function as anion-selective channels that are gated by transitions in the transport cycle.

The ion conduction pathway reported herein accounts for all known functional properties of EAAT/Glt_{Ph} anion channels.

Simulations reveal unitary current amplitudes and ion selectivities (Figures 3C and 3D) that resemble experimental results (Melzer et al., 2003; Wadiche and Kavanaugh, 1998). The calculated minimum pore diameter of Glt_{Ph} is ~5.6 Å (Figure 3E), which perfectly fits the predicted minimum pore diameter of >5 Å based on anion substitution experiments on EAAT1 anion channels (Wadiche and Kavanaugh, 1998). Rapid substrate application experiments have shown that EAAT anion channel activation is delayed compared with glutamate translocation (Grewer et al., 2000). These findings indicate that anion-conducting states existing "outside" the glutamate uptake cycle can be explained by channel opening as a branching reaction from ICs (Figure 1). Simulations predict voltage independence of anion channel opening within the physiological voltage range (Figure 2B). This result explains the experimental observation that the voltage- and substrate dependence of EAAT anion channels are tightly linked to transitions within the transport cycle (Bergles et al., 2002; Machtens et al., 2011a). Simulated anion permeation is unchanged in both the presence and absence of bound substrate (Figure 3E), as expected from the experimental unitary conductances being indistinguishable in the presence and absence of glutamate (Kovermann et al., 2010). Because anion channel opening is tightly linked to translocation of the transport domain, our results indicate that transport substrates increase EAAT anion currents by promoting intermediate states. Distinct EAAT isoforms differ strongly in the relative amplitudes of their transport and anion currents (Fairman et al., 1995; Mim et al., 2005). However, analysis of unitary current amplitudes revealed similar single-channel amplitudes (Schneider et al., 2014; Torres-Salazar and Fahlke, 2007). The high degree of conservation of pore-forming residues (Figure S4) is consistent with the similarities in anion channel unitary current amplitudes and selectivity of different transporter isoforms. Lastly, the novel anion conducting conformation can account for all published mutagenesis and crosslinking results on EAAT anion conduction (Ryan et al., 2004; Shabaneh et al., 2014).

The "S65 path" (Figure S7) is the only location of the anion channel that has been discussed in recent years. We could not find any indication for a direct contribution of this region to anion permeation. Our simulations show that the "S65 path" is hydrated in ChC, thereby suggesting that S65 and adjacent residues could be involved in facilitating the opening of the transport/trimerization domain interface instead. We thus speculate that the "S65 path" may modulate formation of the ChC conformation, which provides an explanation for the impact of mutations in this region on anion channel function (Cater et al., 2014; Ryan and Mindell, 2007; Ryan et al., 2004).

The positive electrostatic potential necessary for perfect anion selectivity of EAAT/Glt_{Ph} anion channels is provided by a single positively charged side chain, R276. Surprisingly, during evolution, this arginine has moved from the tip of HP1 in Glt_{Ph} to TM8 in EAATs, while retaining a similar side chain position in the tertiary structure. In Glt_{Ph}, as well as in EAATs, this arginine has been implicated in binding amino acid substrates, as well as binding Na^+ and K^+ (Ryan et al., 2010; Verdon et al., 2014). Unitary anion conductance is not affected by aspartate (Figure 3), indicating that the interaction of R276 with transport substrates does not modify its effect on anion conduction and selectivity.

The tight linkage between anion channel gating and glutamate transport in EAAT/Glt_{Ph} was previously explained by assuming that certain states of the transport cycle are anion conducting (Bergles et al., 2002). Because Glt_{Ph} structures did not exhibit an open pore with dimensions that might account for the experimentally observed anion conduction properties, it was recently suggested that additional yet to be defined ICs that occur during translocation might be anion conducting (Cater et al., 2014). We have now demonstrated that intermediate transport conformations are nonconducting and that EAAT/Glt_{Ph} anion channel opening transitions require the lateral movement of the glutamate transport domain together with pore hydration from intermediates. Anion channel opening is therefore not part of the transport cycle, but instead is achieved via a branching conformational change. This design permits rapid transition through the full transport cycle without anion channel opening. Furthermore, it allows certain EAAT isoforms to function as effective transporters, with low anion channel open probabilities, and other isoforms to have low transport rates but high occupations of the anion channel mode.

The unique mechanism of EAAT anion channel gating results in neuronal or glial anion conductances that follow changes in substrate concentrations and thus allow feedback control of glutamate release (Wersinger et al., 2006) or modification of GABAergic postsynaptic currents by glutamatergic signals (Winter et al., 2012). Moreover, it explains why isoform-specific variations in glutamate transport by EAATs result in the formation of anion channels that preferentially open or close within their physiological voltage range (Schneider et al., 2014). Recently, gain-of-function mutations in genes encoding EAAT anion channels have been linked to pathological neuronal excitability and cell-volume regulation (Winter et al., 2012). EAAT anion channel activity is also enhanced under conditions of increased synaptic glutamate concentration and may thus contribute to the clinical symptoms associated with brain ischemia or certain neurodegenerative diseases. The structural and mechanistic data presented here might help in the design of EAAT anion channel modulators and thus open therapeutic avenues to correct the cellular defects linked to these pathological conditions.

EXPERIMENTAL PROCEDURES

Molecular Simulations

MD simulations of Glt_{Ph}—bound by a negatively charged aspartate and two Na^+ ions—in outward-facing (OFC; Protein Data Bank [PDB] ID code 2NWX), inward-facing (IFC; PDB ID code 3KBC), and various intermediate conformations (including $IC_{crystal}$; PDB ID code 3V8G) were performed using GROMACS 4.5 (Hess et al., 2008). Based on our OFC and IFC simulation trajectories, we obtained intermediates IC_{int}, IC_{cen}, and IC_{out} from the crystallographic structures of OFC and IFC using essential dynamics sampling simulations (Amadei et al., 1996). Proteins were inserted and equilibrated in a double dimyristoyl phosphatidylcholine bilayer surrounded by a 1 M NaCl aqueous solution and were subjected to various membrane potentials using the computational electrophysiology scheme described recently (Kutzner et al., 2011).

Molecular Biology

Mutant constructs of Glt_{Ph}, human EAAT4, and rat EAAT2 were generated using the QuikChange Site-Directed Mutagenesis Kit (Agilent Technologies) and verified by restriction analysis and DNA sequencing.

Fluorescence Spectroscopy

Fluorescence emission spectra of single-tryptophan Glt_{Ph} mutants in n-dodecyl-β-D-maltoside micelles in the presence of saturating [Na^+] and [Asp^-] at various [I^-] were recorded after excitation at 295 nm. Fluorescence lifetimes were determined through time-correlated single-photon counting.

Electrophysiology

Heterologous expression and whole-cell patch-clamp recordings of EAAT2 and EAAT4 were performed as described previously (Machtens et al., 2011a). Unitary conductances were determined by nonstationary noise analysis of current responses to 300 repetitive voltage jumps to ±150 mV using 140 mM NO_3^- as main anion and 1 mM aspartate as substrate to enhance voltage-dependent gating of the channel.

Statistics

Asterisks indicate the level of statistical significance derived from a two-tailed t test (*** $p < 0.001$; ** $p < 0.01$; * $p < 0.05$; ns, $p \geq 0.05$; see Table S1).

SUPPLEMENTAL INFORMATION

Supplemental Information includes Extended Experimental Procedures, seven figures, one table, and one movie and can be found with this article online at http://dx.doi.org/10.1016/j.cell.2014.12.035.

AUTHOR CONTRIBUTIONS

J.-P.M. and Ch.F. designed the research; J.-P.M. carried out MD simulations; J.-P.M., P.K., and B.B. generated mutant DNA constructs; J.-P.M., D.K., and A.L. performed patch-clamp recordings; C.L. and D.E. conducted fluorescence spectroscopy measurements; J.-P.M. and D.E. analyzed data; B.L.d.G., R.B., and U.Z. advised on the setup and analysis of MD simulations; and J.-P.M., D.E., R.B., B.L.d.G., and Ch.F. prepared the figures and wrote the paper.

ACKNOWLEDGMENTS

These studies were supported by the Deutsche Forschungsgemeinschaft (FA301/9 to Ch.F.; SFB803 to B.L.d.G. and R.B.). The authors gratefully acknowledge the computing time granted on the supercomputer JUROPA at Jülich Supercomputing Centre (JSC) and on the HLRN-II supercomputer of the North-German Supercomputing Alliance (HLRN). We thank A. Alekov, K. Benndorf, H. Grubmüller, and P. Hidalgo for critically reading the manuscript; T. Becher, R.E. Guzman, P. Kovermann, G. Stölting, B. Wilhelm, T. Gensch, I. Weyand, D. Köpfer, D. Wojciechowski, and D.J. Slotboom for helpful discussions; and T. Wassmann for preliminary simulations.

Received: May 23, 2014
Revised: August 27, 2014
Accepted: December 19, 2014
Published: January 29, 2015

REFERENCES

Akyuz, N., Altman, R.B., Blanchard, S.C., and Boudker, O. (2013). Transport dynamics in a glutamate transporter homologue. Nature *502*, 114–118.

Amadei, A., Linssen, A.B.M., de Groot, B.L., van Aalten, D.M.F., and Berendsen, H.J.C. (1996). An efficient method for sampling the essential subspace of proteins. J. Biomol. Struct. Dyn. *13*, 615–625.

Bergles, D.E., Tzingounis, A.V., and Jahr, C.E. (2002). Comparison of coupled and uncoupled currents during glutamate uptake by GLT-1 transporters. J. Neurosci. *22*, 10153–10162.

Boudker, O., Ryan, R.M., Yernool, D., Shimamoto, K., and Gouaux, E. (2007). Coupling substrate and ion binding to extracellular gate of a sodium-dependent aspartate transporter. Nature *445*, 387–393.

Cater, R.J., Vandenberg, R.J., and Ryan, R.M. (2014). The domain interface of the human glutamate transporter EAAT1 mediates chloride permeation. Biophys. J. *107*, 621–629.

Crisman, T.J., Qu, S., Kanner, B.I., and Forrest, L.R. (2009). Inward-facing conformation of glutamate transporters as revealed by their inverted-topology structural repeats. Proc. Natl. Acad. Sci. USA *106*, 20752–20757.

Erkens, G.B., Hänelt, I., Goudsmits, J.M., Slotboom, D.J., and van Oijen, A.M. (2013). Unsynchronised subunit motion in single trimeric sodium-coupled aspartate transporters. Nature *502*, 119–123.

Fairman, W.A., Vandenberg, R.J., Arriza, J.L., Kavanaugh, M.P., and Amara, S.G. (1995). An excitatory amino-acid transporter with properties of a ligand-gated chloride channel. Nature *375*, 599–603.

Grewer, C., Watzke, N., Wiessner, M., and Rauen, T. (2000). Glutamate translocation of the neuronal glutamate transporter EAAC1 occurs within milliseconds. Proc. Natl. Acad. Sci. USA *97*, 9706–9711.

Grewer, C., Balani, P., Weidenfeller, C., Bartusel, T., Tao, Z., and Rauen, T. (2005). Individual subunits of the glutamate transporter EAAC1 homotrimer function independently of each other. Biochemistry *44*, 11913–11923.

Groeneveld, M., and Slotboom, D.J. (2010). Na^+:aspartate coupling stoichiometry in the glutamate transporter homologue Glt_{Ph}. Biochemistry *49*, 3511–3513.

Hess, B., Kutzner, C., van der Spoel, D., and Lindahl, E. (2008). GROMACS 4: algorithms for highly efficient, load-balanced, and scalable molecular simulation. J. Chem. Theory Comput. *4*, 435–447.

Jensen, M.O., Jogini, V., Borhani, D.W., Leffler, A.E., Dror, R.O., and Shaw, D.E. (2012). Mechanism of voltage gating in potassium channels. Science *336*, 229–233.

Kanner, B.I., and Sharon, I. (1978). Active transport of L-glutamate by membrane vesicles isolated from rat brain. Biochemistry *17*, 3949–3953.

Kovermann, P., Machtens, J.P., Ewers, D., and Fahlke, C. (2010). A conserved aspartate determines pore properties of anion channels associated with excitatory amino acid transporter 4 (EAAT4). J. Biol. Chem. *285*, 23676–23686.

Kutzner, C., Grubmüller, H., de Groot, B.L., and Zachariae, U. (2011). Computational electrophysiology: the molecular dynamics of ion channel permeation and selectivity in atomistic detail. Biophys. J. *101*, 809–817.

Lakowicz, J.R. (2006). Principles of fluorescence spectroscopy. In Principles of Fluorescence Spectroscopy, P.H. Lakowicz, ed. (New York: Springer), pp. 529–575.

Machtens, J.P., Kovermann, P., and Fahlke, C. (2011a). Substrate-dependent gating of anion channels associated with excitatory amino acid transporter 4. J. Biol. Chem. *286*, 23780–23788.

Melzer, N., Biela, A., and Fahlke, C. (2003). Glutamate modifies ion conduction and voltage-dependent gating of excitatory amino acid transporter-associated anion channels. J. Biol. Chem. *278*, 50112–50119.

Mim, C., Balani, P., Rauen, T., and Grewer, C. (2005). The glutamate transporter subtypes EAAT4 and EAATs 1-3 transport glutamate with dramatically different kinetics and voltage dependence but share a common uptake mechanism. J. Gen. Physiol. *126*, 571–589.

Otis, T.S., and Kavanaugh, M.P. (2000). Isolation of current components and partial reaction cycles in the glial glutamate transporter EAAT2. J. Neurosci. *20*, 2749–2757.

Picaud, S.A., Larsson, H.P., Grant, G.B., Lecar, H., and Werblin, F.S. (1995). Glutamate-gated chloride channel with glutamate-transporter-like properties in cone photoreceptors of the tiger salamander. J. Neurophysiol. *74*, 1760–1771.

Reyes, N., Ginter, C., and Boudker, O. (2009). Transport mechanism of a bacterial homologue of glutamate transporters. Nature *462*, 880–885.

Ryan, R.M., and Mindell, J.A. (2007). The uncoupled chloride conductance of a bacterial glutamate transporter homolog. Nat. Struct. Mol. Biol. *14*, 365–371.

Ryan, R.M., Mitrovic, A.D., and Vandenberg, R.J. (2004). The chloride permeation pathway of a glutamate transporter and its proximity to the glutamate translocation pathway. J. Biol. Chem. *279*, 20742–20751.

Ryan, R.M., Kortt, N.C., Sirivanta, T., and Vandenberg, R.J. (2010). The position of an arginine residue influences substrate affinity and K^+ coupling in the human glutamate transporter, EAAT1. J. Neurochem. *114*, 565–575.

Schneider, N., Cordeiro, S., Machtens, J.P., Braams, S., Rauen, T., and Fahlke, C. (2014). Functional properties of the retinal glutamate transporters GLT-1c and EAAT5. J. Biol. Chem. *289*, 1815–1824.

Shabaneh, M., Rosental, N., and Kanner, B.I. (2014). Disulfide cross-linking of transport and trimerization domains of a neuronal glutamate transporter restricts the role of the substrate to the gating of the anion conductance. J. Biol. Chem. *289*, 11175–11182.

Shrivastava, I.H., Jiang, J., Amara, S.G., and Bahar, I. (2008). Time-resolved mechanism of extracellular gate opening and substrate binding in a glutamate transporter. J. Biol. Chem. *283*, 28680–28690.

Torres-Salazar, D., and Fahlke, C. (2007). Neuronal glutamate transporters vary in substrate transport rate but not in unitary anion channel conductance. J. Biol. Chem. *282*, 34719–34726.

Vaitheeswaran, S., Rasaiah, J.C., and Hummer, G. (2004). Electric field and temperature effects on water in the narrow nonpolar pores of carbon nanotubes. J. Chem. Phys. *121*, 7955–7965.

Vázquez-Ibar, J.L., Guan, L., Weinglass, A.B., Verner, G., Gordillo, R., and Kaback, H.R. (2004). Sugar recognition by the lactose permease of Escherichia coli. J. Biol. Chem. *279*, 49214–49221.

Verdon, G., and Boudker, O. (2012). Crystal structure of an asymmetric trimer of a bacterial glutamate transporter homolog. Nat. Struct. Mol. Biol. *19*, 355–357.

Verdon, G., Oh, S., Serio, R.N., and Boudker, O. (2014). Coupled ion binding and structural transitions along the transport cycle of glutamate transporters. eLife *3*, e02283.

Wadiche, J.I., and Kavanaugh, M.P. (1998). Macroscopic and microscopic properties of a cloned glutamate transporter/chloride channel. J. Neurosci. *18*, 7650–7661.

Wersinger, E., Schwab, Y., Sahel, J.A., Rendon, A., Pow, D.V., Picaud, S., and Roux, M.J. (2006). The glutamate transporter EAAT5 works as a presynaptic receptor in mouse rod bipolar cells. J. Physiol. *577*, 221–234.

Winter, N., Kovermann, P., and Fahlke, C. (2012). A point mutation associated with episodic ataxia 6 increases glutamate transporter anion currents. Brain *135*, 3416–3425.

Yernool, D., Boudker, O., Jin, Y., and Gouaux, E. (2004). Structure of a glutamate transporter homologue from Pyrococcus horikoshii. Nature *431*, 811–818.